Performance of Floating Point Absorbers attached to a Breakwater and Effect of Control Strategies

Markos Bonovas, Alexandros Magkouris, and Kostas Belibassakis

Abstract— **The estimation of the performance of Wave Energy Converter (WEC) arrays of the type of simple floaters operating in nearshore and coastal areas, characterized by variable bottom topography, is important for the estimation of the wave power absorption and determination of the operational characteristics of the system and could significantly contribute to the efficient design and layout of WEC farms. For this purpose, full 3D models based on Boundary Element Method have been developed, supporting the systematic use for optimization studies. Apart from WEC arrays in nearshore and coastal regions a promising possibility is the installation at the exposed side of port breakwaters with significant energy potential. In this work, the analysis of the above system is extended to the prediction of WEC performance in multichromatic incident waves under latching control strategy using a time-domain simulator, showing improvement of performance in particular conditions.**

Keywords—**Breakwater, Point Absorber, Time Domain, Wave Energy.**

I. Introduction

MARINE renewable energy sources support sustainable energy transition and decarbonization. Wave Energy Converters (WECs) deployed in nearshore and coastal areas significantly contribute to harnessing of wave energy, with the point-absorber type being one of the most prevailing systems. In this direction, the assessment of WECs performance is crucial for the evaluation of wave power absorption, as well as the definition of optimized structural and functional parameters and plays a decisive role towards the efficient design and layout of WEC farms. Coastal areas are characterized by variable bottom topography and, as pointed out in Ref. [1], this could affect their design and performance, even in a constructive way. As evaluated in Ref. [1] by using suitably developed tools, this effect is quantified and the methodology, due to its relatively low computational cost, could be used for basic research and design purposes in terms of wave farms [2], [3], [4]. Moreover, WEC arrays have been recently considered for installation on the exposed side of breakwaters or piers, as shown in Figs.1,2, which offers some advantages concerning the improvement of performance, as well as installation and maintenance of the devices. Recently, such deployments have been made in areas of increased wave potential as shown in Fig.3.

In previous works by the authors [5] a simplified model based on the Modified Mild-Slope Equation, in conjunction with 3D floating body hydrodynamic simulators (e.g., [6], [7], for more details), is developed for modelling the scattering of waves from multiple heaving point absorbers arranged in an array in general bottom topography, supporting optimal design studies.

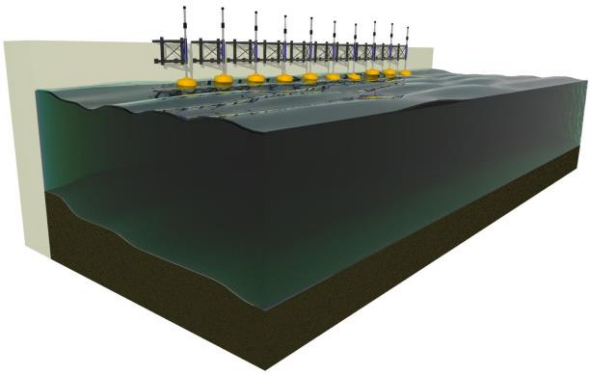

Fig. 1. WECs attached to vertical wall (iso view).

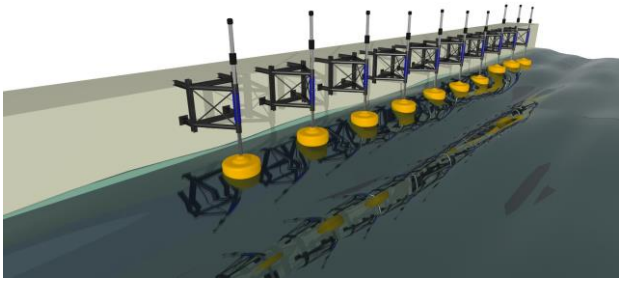

Fig. 2. WECs attached to vertical wall (exposed side of breakwater).

M. B. is PhD student at the School of Naval Architecture and marine Engineering of National Technical University of Athens (e-mail: markosbonovas@hotmail.gr).

A. M. is PhD student at the School of Naval Architecture and marine Engineering of National Technical University of Athens (e-mail: alexmagouris@gmail.com).

K. B. is Professor of the School of Naval Architecture and marine Engineering of National Technical University of Athens (e-mail: kbel@fluid.mecech.ntua.gr).

Digital Object Identifier: https://doi.org/10.36688/ewtec-2023-538

Fig. 3. Installation of WECs at the breakwater of the port of Heraklion, Crete island, Greece.

The above technique is restricted to the case of heaving point absorbers and its novelty lies in the development of an analytical model for the scattered and dissipated wave fields by circular inclusions on the horizontal plane, obtained by the Helmholtz equation, to which the MMSE is transformed [5]. Wave power extraction effects are modelled by means of suitable absorbing coefficients calibrated by correlating the energy loss due to artificial absorption with the power output of floating heaving bodies of general shape in constant depth, calculated by local 3D BEM solvers [8], [9], taking also into account the WEC Power Take Off effect, modelled by an additional damping coefficient in the system dynamics. The BEM methodology is validated against analytical solutions whenever possible and used for optimization studies in terms of WEC design (e.g. WEC shape, Power Take-Off aspects etc.). The method is also extended to six degrees of freedom for the body and is able to simulate effects caused by steep depth variations; see [10].

In this work the method is extended to implement additional features. Specifically, reflection effects are included in the BEM solver, assuming the deployment of a device at the exposed side of a port breakwater. Moreover, another crucial aspect of wave absorbing devices technology is addressed: control. Latching technique is used in order to maximize the power output of the device, by constraining some of the operational characteristics. The dynamic behaviour of the WEC is at first obtained in the frequency-domain and the solution is subsequently transferred in the time-domain. A simulator is then applied for the prediction of a single WEC performance under latching control strategy.

II. MATHEMATICAL FORMULATION

A. 3D-BEM for the Analysis of WECs with Wall Effects

Considering a (single DoF) heaving Point Absorber WEC attached to the exposed side of a breakwater, operating in constant local depth h and subjected to harmonic wave excitation, the magnitude of its heave

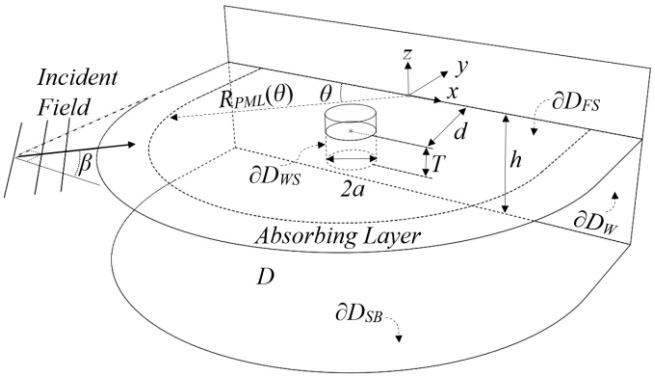

Fig. 4. Sketch of the considered configuration, illustrating the basic dimensions and the various parts of the flow field boundary.

oscillation is derived by the analysis of the surrounding flow field in the domain D (see Fig.4).

Following standard floating body hydrodynamic theory, the flow field is decomposed into the incident, the diffracted and the radiated subfields. The velocity field of each of the above is represented by the gradient of the corresponding potential function $\Phi_0(\mathbf{x};t)$, $\Phi_d(\mathbf{x};t)$, and $\Phi_3(\mathbf{x};t)$. The coordinate system $\mathbf{x} = (x, y, z)$ is used, with the origin placed at Mean Water Level (MWL), at the position of the vertical wall, so that the center of the WEC's waterplane area is located at $(x, y) = (0, -d)$ as schematically shown in Fig.4. The above interaction problem is treated in the frequency domain using the representation:

$$\Phi(\mathbf{x};t) = \mathrm{Re}\left\{-\frac{igA}{\omega}\varphi(\mathbf{x})\cdot\exp(-i\omega t)\right\}, \tag{1}$$

where A is the incident wave amplitude, g is the acceleration due to gravity, ω is the angular frequency, i is the imaginary unit and $\varphi(\mathbf{x})$ is the complex potential in the frequency domain, which equals:

$$\varphi(\mathbf{x}) = -i\omega\left\{\varphi_0(\mathbf{x}) + \varphi_d(\mathbf{x}) + \xi_3\varphi_3(\mathbf{x})\right\}, \tag{2}$$

where $\varphi_k, k = 0, d, 3$, stand for the complex amplitudes of each subfield and ξ_3 denotes the complex amplitude of the WEC's oscillation in the z-direction. For simplicity, in this work, a cylindrical WEC shape of radius a and draft T is considered. However, the methodology presented is trivially extendable to any other axisymmetric or arbitrary device geometry.

The complex potential of the incident field, incorporating the reflection effects due to the vertical wall's presence, is assumed to be known and for A=1 equals:

$$\varphi_0(\mathbf{x}) = \frac{g}{\omega^2}\frac{\cosh\left(k\left[z+h\right]\right)}{\cosh(kh)}F(x,y,\beta), \tag{3a}$$

where

$$F(x,y,\beta) = \exp\left(ik\left(\cos(\beta)x + \sin(\beta)y\right)\right) + R\exp\left(ik\left(\cos(-\beta)x + \sin(-\beta)y\right)\right). \tag{3b}$$

In the above equations β is the direction of propagation and R is a reflection coefficient, which takes the value R=0 to eliminate the reflection of the incident field in case of propagation parallel to the wall (β=0° or β=180°), or the value R=1 to generate the reflected field, otherwise. Additionally, the parameter k in (3) denotes the wavenumber, calculated as the real root of the linear dispersion relation:

$$\omega^2 = k\, g \tanh(kh) \tag{4}$$

The diffraction and radiation subfields are evaluated by suitably defined Boundary Value Problems (BVPs), governed by the Laplace equation, while appropriate Boundary Conditions (BCs) are satisfied at the various parts of the boundary ∂D of the flow domain, which consists of the free surface of the water (∂D_{FS}), the wetted surface of the WEC (∂D_{WS}) and the impermeable boundaries of the wall (∂D_W) and the seabed (∂D_{SB}), see also Fig.4. Impermeability BCs apply to the solid boundaries while the linearized Free Surface Boundary Condition (FSBC) applies to the free surface of the water at z=0. Specifically, the diffracted and radiated fields are obtained as solutions to the following BVPs for $k=d, 3$:

$$\nabla^2 \varphi_k(\mathbf{x}) = 0,\ \mathbf{x} \in D, \tag{5a}$$

$$\frac{\partial \varphi_k(\mathbf{x})}{\partial n} - \mu(\mathbf{x};\omega)\varphi_k(\mathbf{x}) = 0,\ \mathbf{x} \in \partial D_{FS}, \tag{5b}$$

$$\frac{\partial \varphi_k(\mathbf{x})}{\partial n} = N_k(\mathbf{x}),\ \ \mathbf{x} \in \partial D_{WS}, \tag{5c}$$

$$\frac{\partial \varphi_k(\mathbf{x})}{\partial n} = 0,\ \ \mathbf{x} \in (\partial D_{SB} \cup \partial D_W). \tag{5d}$$

In the above equations, $\mathbf{n} = (n_1, n_2, n_3)$ is the unit vector normal to ∂D, directed toward the exterior of D and the boundary data involved in (5c) are defined as follows:

$$N_d(\mathbf{x}) = -\frac{\partial \varphi_0(\mathbf{x})}{\partial n} \ \text{ and } \ N_3(\mathbf{x}) = n_3(\mathbf{x}) \tag{6}$$

Moreover, $\mu = \omega^2/g$ is the frequency parameter, which is modified as explained in the sequel. In order to eliminate the infinite extent of the domain, a Perfectly Matched Layer (PML) technique is adopted, consisting of an absorbing layer which is used to attenuate the outgoing wave solutions in an optimal way and treat the radiating behaviour of the diffraction and radiation fields at far distances from the WEC, preventing reflections from the outer boundary [1] (see also Fig.4). The efficiency of this technique in damping outgoing waves with minimal reflection depends on the thickness of the layer, which is taken to be of the order of 1 characteristic wavelength $\lambda = 2\pi/k$, while its coefficient is taken increasing within the layer. Implementation of the PML technique is achieved by making the frequency parameter complex inside the layer to approximate artificial weakening of the wave solutions. Specifically, the frequency parameter is redefined as, follows:

$$\mu(\mathbf{x};\omega) = \begin{cases} \omega^2 g^{-1}, & |\mathbf{x}| < R_{PML}[\theta(\mathbf{x})] \\ \omega^2 g^{-1}\left(1 + P(\mathbf{x})\right)^2, & |\mathbf{x}| \geq R_{PML}[\theta(\mathbf{x})] \end{cases} \tag{7a}$$

where

$$P(\mathbf{x}) = ic\frac{\left(|\mathbf{x}| - R_{PML}[\theta(\mathbf{x})]\right)^n}{\lambda^n}. \tag{7b}$$

In the above equations $R_{PML}[\theta(\mathbf{x})]$ denotes the PML activation radius in the direction $\theta(\mathbf{x}) = tan^{-1}(y/x)$. As shown in Fig.4, the PML is activated on a curve defined on the MWL plane by a semicircle centred at (x,y)=$(0,-d)$ supplemented by two straight lines of length d. The parameter c and the exponent n are used as optimized in in previous works [9], aiming to the maximization of the layer's efficiency, preventing numerical reflections and not contaminating the evaluated fields.

The BVPs described by Eqs. (5) are treated by means of a low-order panel method, based on simple singularity distributions and 4-node quadrilateral boundary elements, ensuring continuity of the geometry of the various parts of the boundary [8], [9]. The complex potential functions $\varphi_k, k = d, 3$, are represented by

$$\varphi_k(\mathbf{x}) = \int_{\partial D} \sigma_k(\mathbf{x}') \cdot G(\mathbf{x}'|\mathbf{x}) dS(\mathbf{x}'),\ \ \mathbf{x} \in D, \mathbf{x}' \in \partial\widehat{D}, \tag{8}$$

where $\partial\widehat{D}$ denotes the boundary of D, excluding the seabed part (∂D_{SB}), while the homogeneous Neumann BC on the latter part is taken into account by using the following Green's function for the Laplace equation in 3D in (8):

$$\hat{G}(\mathbf{x}'|\mathbf{x}) = G(\mathbf{x}'|\mathbf{x}) + G(\mathbf{x}'|\hat{\mathbf{x}}), \tag{9}$$

which involves the contribution by the mirror point $\hat{\mathbf{x}} = (x, y, -2h - z)$ with respect to the horizontal seabed plane: $z = -h$. Furthermore, $\sigma_k(\mathbf{x}'), k = d, 3$ are singularity strength distributions, defined on the boundary $\partial\widehat{D}$. These distributions are evaluated by the low order panel method, under the assumption of being piecewise constant on each element and, in conjunction with a discretized form of (8), they reproduce the subfields $\varphi_k, k = d, 3$.

The above potentials and corresponding velocity fields are approximated by:

$$\varphi(\mathbf{x}) = \sum_p \sigma_p \Phi_p(\mathbf{x}),\ \nabla\varphi(\mathbf{x}) = \sum_p \sigma_p \mathbf{U}_p(\mathbf{x}) \tag{10}$$

where the summation ranges over all panels, indexed by p, σ_p is the singularity distribution's strength on the p-th element while Φ_p and $\mathbf{U}_p$, respectively, denote induced potential and velocity from the p-th element with unit singularity distribution to the field point $\mathbf{x}$ with more details in[11].

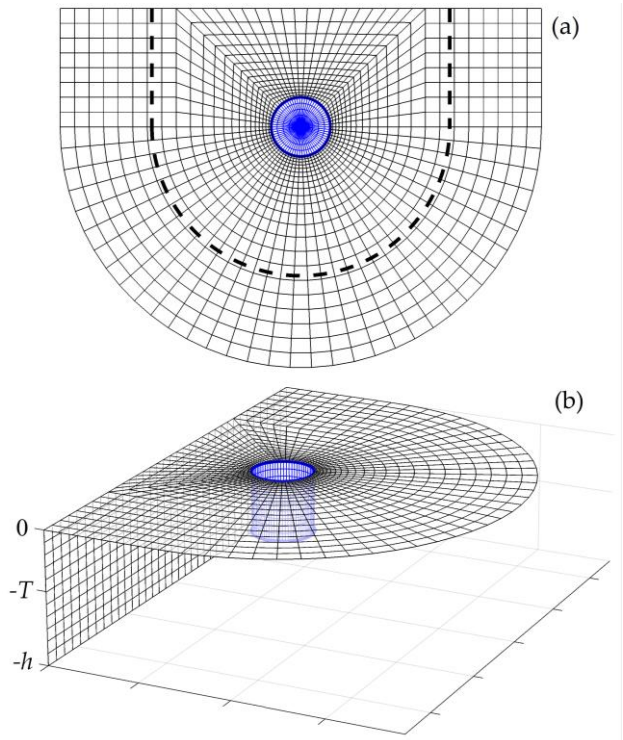

Fig. 5. Indicative boundary mesh of $\partial\hat{D}$. (a) top view with PML activation curve marked by a dashed line. (b) 3D view.

The numerical solutions are obtained using a collocation method, satisfying each BC at the centroid of the corresponding panels on the various parts of the boundary (i.e., wetted surface, free surface, wall), while the no-entrance condition is satisfied everywhere on z=-h. Using constant normal dipole distributions on each quadrilateral panel, the matrix of induced potential is analytically calculated via the solid angle [12]. Moreover, using the equivalence of a constant dipole element to a vortex ring element, the calculation of induced velocity is obtained by repetitively applying the Biot–Savart law. As concerns discretization, a minimum of 15-20 elements per wavelength is required in discretizing the free surface in order to eliminate numerical errors due to damping and dispersion associated with the above numerical scheme.

An important aspect of the BEM formulation is the mesh generation. The discretization is accomplished by incorporating corresponding meshes on the various boundary surfaces and an important feature is the continuous junctions between the different parts of the mesh, which, in conjunction with the quadrilateral elements, ensures global continuity of the boundary.

A plot of the boundary mesh is presented in Fig.5 where it can be seen that increased grid resolution is applied to the near field and on the wetted surface of the WEC for obtaining better quality results. Moreover, Fig.6 illustrates plots of the calculated free surface elevation corresponding to the incident (a, c, e) and the diffracted (b, d, f) fields, in the case of incident waves of frequency $\tilde{\omega} = \omega\sqrt{\alpha/g} = 1$, in water depth. h=0.7 m, for propagation direction β=0°(a, b), β=30° (c, d) and β=90°(e, f).

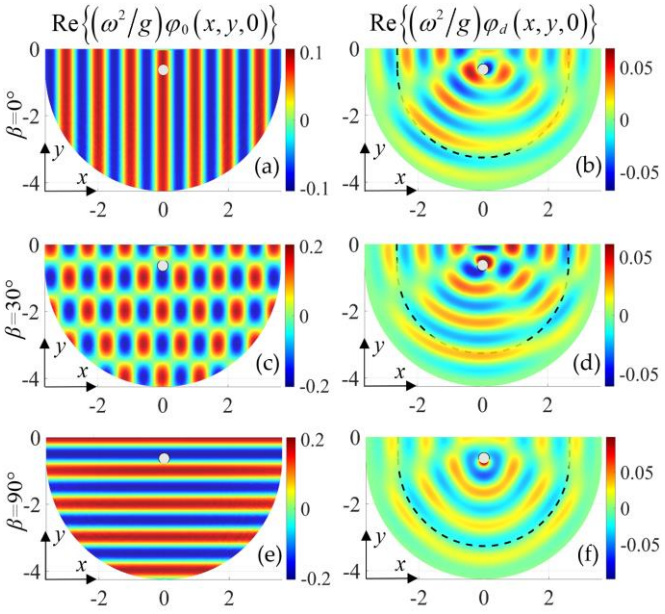

Fig. 6. Real part of calculated free surface elevation corresponding to the incident (a, c, e) and the diffracted (b, d, f) fields. Propagation direction β=0° (a, b), β=30° (c, d) and β=90° (e, f). h=0.7 m, A=0.1 m. $\omega\sqrt{\alpha/g} = 1$.

Using standard linear theory, we obtain the corresponding heave response of the above WEC as follows:

$$\xi_3 = \left(F_0 + F_d\right)/D\,, \tag{11}$$

where:

$$F_k = \omega^2\rho \int_{\partial D_{WS}} \varphi_k(\mathbf{x})\cdot n_3(\mathbf{x})\,dS(\mathbf{x}),\ x \in \partial D_{WS},\ k = 0, d\,, \tag{12}$$

are the vertical Froude-Krylov (FK) and diffraction forces acting on the WEC, with ρ denoting the water density, and

$$D = -\omega^2\left(M + A_{33}\right) - i\omega\left(B_{33} + B_{PTO}\right) + C_{33}. \tag{13}$$

In the above Equation, M denotes the mass of the floating body evaluated by the submerged volume times the water density. The added mass and hydrodynamic damping coefficients A_{33} and B_{33} are obtained via the calculated radiation field as:

$$\omega^2 A_{33} + i\omega B_{33} = \rho \int_{\partial D_{WS}} \varphi_3(\mathbf{x})\cdot n_3(\mathbf{x})\,dS(\mathbf{x}), \mathbf{x} \in \partial D_{WS}\,. \tag{14}$$

Moreover, $C_{33} = \rho g \pi \alpha^2$ is the heave hydrostatic coefficient, with α being the WEC radius. Finally, B_{PTO} models the extraction of energy from the Power Take-Off system, which is achieved by an additional damping coefficient.

The mean output power of the WEC device is then evaluated:

$$P_{OUT} = \frac{1}{2}\eta_{eff}\,\omega^2 B_{PTO}\left|\xi_3\right|^2, \tag{15}$$

where η_{eff} stands for the efficiency of the electromechanical PTO system, and thus the performance

index is defined by normalizing the above result with respect to the incident wave power flux over the cross section of the device, given by the WEC waterline diameter, considering a wave of height $H = 2A$:

$$P = \frac{P_{OUT}}{0.25\rho g H^2 C_g a}. \quad (16)$$

III. RESULTS

Numerical results are presented hereupon for the case of a cylindrical WEC installed in an area of water depth h with $\alpha/h = 0.225$, $T/h = 0.45$ and $d/a = 4$.

In the absence of data concerning values of η_{eff}, numerical results for the cylindrical WEC are obtained and presented using the present BEM for $\eta_{eff} = 1$. Moreover, representative values for B_{PTO} are used in the form: $B_{PTO}=j\,B_{33,av}$ where $B_{33,av}$ denotes a characteristic value obtained as the frequency average of the calculated hydrodynamic damping coefficient B_{33}, and j is a multiplying factor, defined as j=[5,10,20]. In addition, the case B_{PTO}=0 is considered corresponding to the freely floating body.

Different angles of incidence of 0°,30°, 45°, 60° and 90° are considered, with 0° and 90° being referential cases as parallel wavefront propagation and normal incidence to the wall (resulting to standing waves), respectively. Visual examples of the incident and the diffracted wave fields are provided in Fig.6, as regards propagation at 0°, 30° and 90°, at depth $h = 0.7$m and with the non-dimensional frequency $\tilde{\omega} = \omega\sqrt{\alpha/g}$ set to unit value. The subplots show the real part of the incident and diffracted potentials, multiplied by (ω^2/g) so as to represent the free surface elevation $\eta(x, y)$, showing how the field is transformed based on the direction of propagation.

The Froude-Krylov and diffraction forces, normalized with respect to ($\rho g \pi A \alpha^2$), and the WEC's heave Response Amplitude Operators (RAOs), for B_{PTO}=0, are depicted in Figs.7(a), 7(b) and 8 respectively, showing a turning point in the WEC's behaviour due to wall-induced effects. Non-dimensional added mass and hydrodynamic damping coefficients, as calculated by (14), are plotted in Fig.9. For comparison, in Fig.9 corresponding results are plotted in the absence of the vertical wall (open sea). The latter results can be obtained either by eliminating the wall and extending the free surface and the PML in all directions in the previous numerical scheme, or by an available analytical solution, discussed in the sequel.

It is observed that in case of incident angles lower than 90°, the wall has a constructive effect to the device's vertical motion, with the bounce-back of the wave enhancing the efficiency of the whole layout. In 90° propagation standing waves occur, thus heave response strongly depends on wavelength and whether the WEC is located on a node or an antinode of the incident field.

As per previous description and for propagation angles of 0° and 30°, Heave RAO of the WEC is plotted in Fig.10 for the three different PTO values.

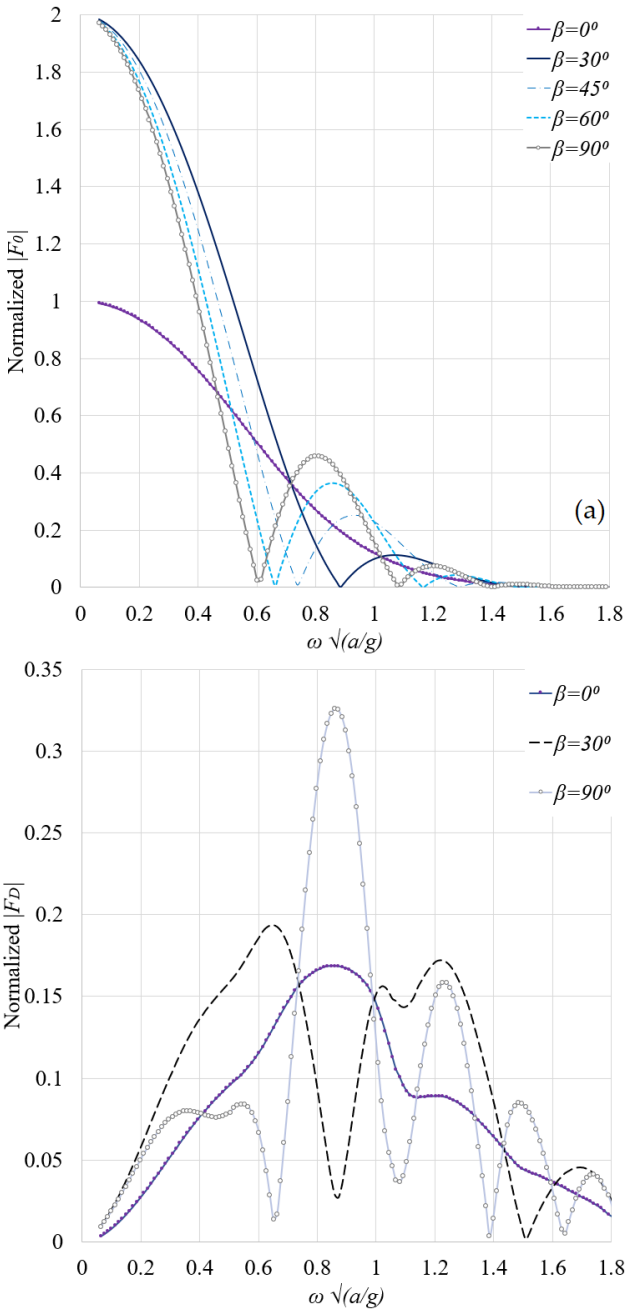

Fig. 7. Normalized Vertical Forces for Cyl-WEC α/h=0.225, T/h=0.45, d/a=4. (a) FK-forces, Propagation direction β=[0°,30°,45°,60°,90°], (b) Diffraction forces, Propagation direction β=[0°,30°,90°].

Due to the increase in damping effects, greater values of B_{PTO} lead to flattening of the power output curve, while lower values result to more peaked distributions.

Subsequently, Fig. 11 shows the absorbed power by the device, normalized in relevance to the power of the propagating field. It might be raised that the reflected field should be taken under consideration as well, as available power for absorption by the device. However, this is also a manmade structure and is approached as part of the WEC technology implemented in this case, thus neglected from the denominator of the performance index.

Generally, optimum value of the PTO damping should be determined by an integral-based approach of the normalized power curve, since the area below the curve corresponds to the amount of energy absorbed.

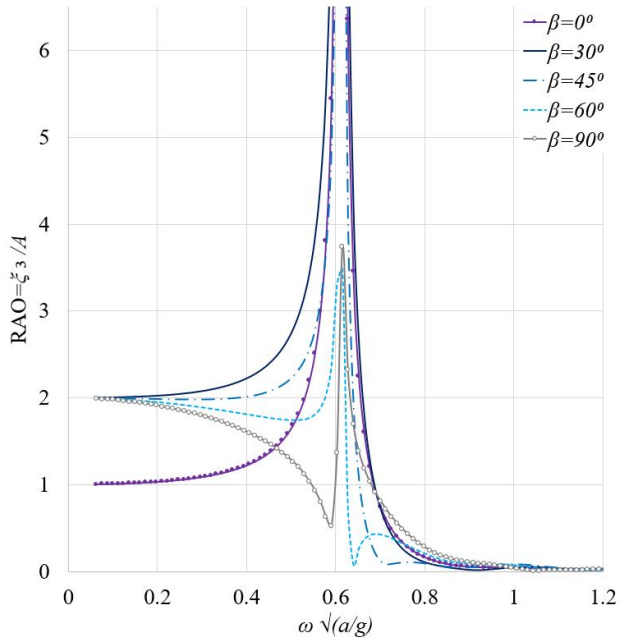

Fig. 8. Heave RAO for Cyl-WEC α/h=0.225, T/h=0.45, d/a=4. Propagation direction β=[0°,30°,45°,60°,90°], B_{PTO}=0

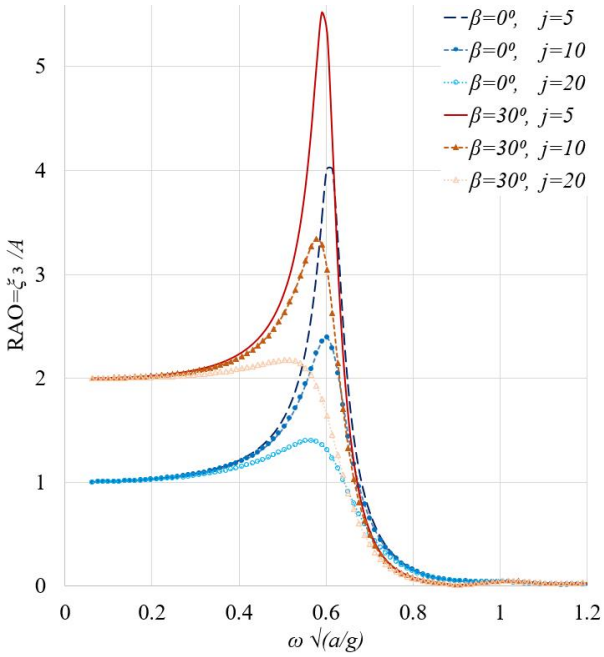

Fig. 10. Heave RAO for Cyl-WEC α/h=0.225, T/h=0.45, d/a=4 and different B_{PTO}=[5,10,20] $B_{33,av}$. Propagation direction β=[0°,30°].

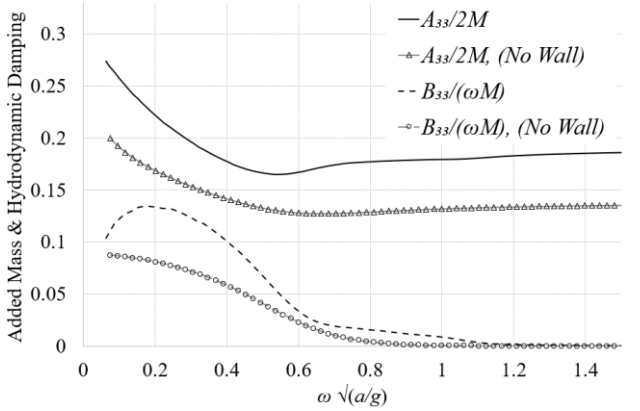

Fig. 9. Added mass and hydrodynamic damping coefficients for Cyl-WEC α/h=0.225, T/h=0.45, d/a=4, and corresponding results in open sea.

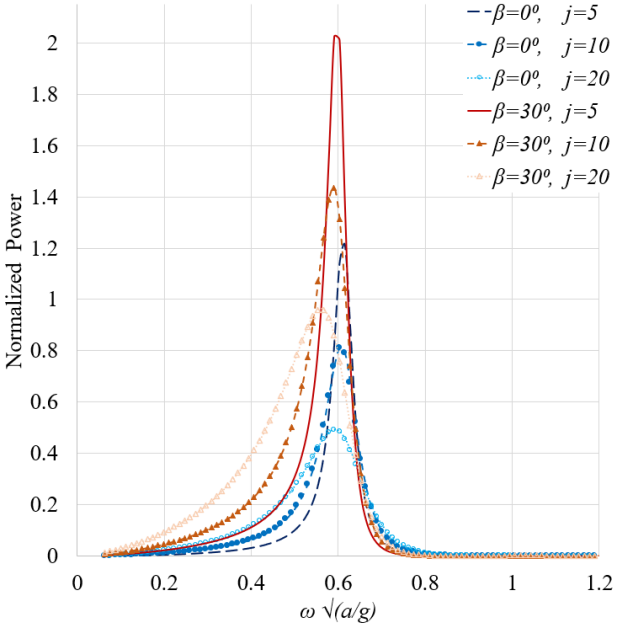

Fig. 11. Normalized Power for Cyl-WEC α/h=0.225, T/h=0.45, d/a=4 and different B_{PTO}=[5,10,20] $B_{33,av}$. Propagation direction β=[0°,30°].

In Fig.11 it is clearly shown that the normalized power achieves values well above one, manifesting the beneficial effect of the wall and quantifying the constructive interaction of fluid and structures.

Overall assessment, sensibly justifies that performance in case of 30° propagation is superior, compared to the case of wave propagation parallel to the wall, since in all cases area below the curves is significantly greater than the ones corresponding to propagation at 0°.

IV. TIME-DOMAIN IMPLEMENTATION OF CONTROL STRATEGY

Control of WECs is one of the aspects of current trends in research and of major significance for the developing industry. By applying such strategies, increased energy amounts could be harnessed by the device.

A common control technique applied to point absorber WECs is the latching. By using a simple clamping mechanism and without requiring significant energy draw from the system, the otherwise freely oscillating body, now has its heave motion constrained, based on values of its velocity and wave induced excitation forces.

Latching is a simple switching, suboptimal "phase" control, aiming to maximize energy absorption by keeping the velocity of the body in phase with the excitation force and it is more efficient when the period of the incoming wave is greater than the resonance period of the WEC. More specifically, the body is latched from the moment when its velocity reaches zero, thus corresponding to its upper and lower dead points. It should be kept latched for

a specific time interval. The definition of this interval is the design variable in optimizing latching control and is strongly dependent on the considered sea spectrum.

Therefore, evaluation of the optimal time interval before unlatching has to be performed. For regular seas, where only monochromatic propagation occurs, it is easily calculated [13]. For irregular seas however, the solution has been a research subject for several years. The empirical approach, as discussed in Ref. [14] is hence being applied. In this approach, the latching interval spans from the time when velocity reaches zero, until a quarter of the resonance period before the next predicted peak of the excitation force. This way, larger peak velocities are obtained and thus larger amount of energy is absorbed by the device. Prediction of the excitation's behaviour is a common bottleneck in terms of control strategies and of course not applicable in a real-time concept, due to its computational cost. However, despite its simplicity, latching control is very effective [15].

Generally, control strategies, including latching, are nonlinearities in the hydrodynamic problem, which should be treated in the time domain. Since previous analysis and computational tools are developed in the frequency-domain the solution has to be "translated" to a time-domain equivalent. Subsequently, numerical iterative methods will be used for the approximation of the solution [16].

In this work, the case of a heaving cylinder will be examined operating at constant depth h and with the free surface extending infinitely in all directions. Therefore, the response does not depend on the angle of propagation which is set to zero.

Furthermore, an analytical approach is used for the evaluation of hydrodynamic coefficients (damping and added mass), and the vertical excitation forces, as presented in Refs. [17], [18], [19], [20]. A Bretschneider sea spectrum is assumed and a random phase model is used to generate spectral excitation data. The considered spectrum is expressed in terms of the angular frequency ω as:

$$S(\omega)=\frac{5}{16}\frac{\omega_p^4}{\omega^5}H_S^2\exp\left[-\frac{5}{4}\left(\frac{\omega_p}{\omega}\right)^4\right] \quad (17)$$

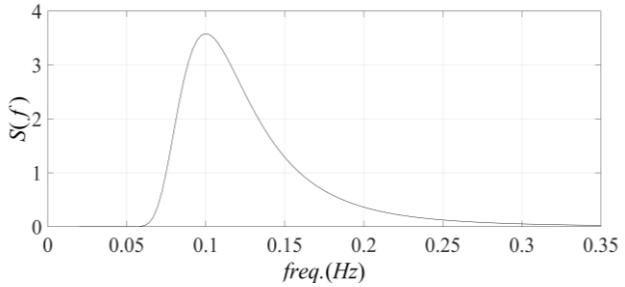

Fig. 12. Bretschneider spectrum used to generate spectral excitation data. $T_p = 10\ s$, $H_S = 2\ m$.

For obtaining quantified results, a spectrum is selected with peak frequency $\omega_p = 2\pi/T_p$, where $T_p = 10\ s$ is the peak period, while the significant wave height is set to $H_S = 2\ m$. The resulting spectrum $S(f) = 2\pi\, S(\omega)$ is illustrated in Fig.12 as a function of the natural frequency $f = 2\pi\ /\omega$.

In particular, the following 2nd Order Differential Equation of Motion is used:

$$\ddot{\xi}_3(t)=\frac{F_{33}(t)-(B_{33}+B_{PTO})\dot{\xi}_3(t)-(C_{33}+C_{PTO})\xi_3(t)}{M+A_{33}} \quad . \quad (18)$$

A Predictor-Corrector Method based on Adam-Bashforth and Adams-Moulton is applied, thus formulating a hybrid algorithm for the numerical approximation of the solution. The four-step Adams-Bashforth (AB) is used for the Prediction and the four-step Adams-Moulton (AM) is used for the Correction. For the Predictor calculation an explicit formula is used, while for the Corrector implicit equation is being solved.

Keeping the general design unchanged from the previous section in terms of non-dimensional variables, the WEC is a cylinder with $a = 4.5\text{m}$, $T = 9\text{m}$, operating in an area of depth $h = 20\text{m}$. The PTO damping is $B_{PTO} = 10 \times B_{33,av} = 6.1 \times 10^4\ Ns/m$, for keeping also consistency with PTO damping values used previously, while the PTO stiffness is $C_{PTO} = 0.1 \times C_{33} = 6.2 \times 10^4\ N/m$, corresponding to magnitudes used in the literature [21]. Approximation of the solution via AB-AM algorithm is performed for a time span of 55 peak periods T_p with time step 0.01s.

Focusing of peak frequencies of the spectrum, the Latching interval is one of the most significant design variables of this optimization problem and is selected as:

$$T_{latch}=\frac{T_p-T_{res}}{2}, \quad (19)$$

where T_p is the peak period of the wave spectrum and T_{res} is the resonance frequency of the WEC [22] . The resonance period of the device is equal to 6.7s. Based on above, the switching mechanism simply keeps the body latched from the moment of zero velocity and for a time interval equal to T_{latch}, which is kept constant, resulting in keeping the velocity in phase with the excitation and achieving higher amounts of wave power harnessed. As concerns the computational algorithm, the latching is simulated by increasing the PTO damping coefficient by a factor of 400 for the considered time interval. Fig.13(a) depicts the heaving Motion of the WEC along with the latching windows, while Fig.13(b) illustrates the corresponding data in a shorter time interval of 1 min which is marked by two dashed lines in Fig.13(a). Finally, Fig.13(c) shows the resulting power absorption as a function of time. As it can be seen in Fig.13 latching control is applied starting from t=250s.

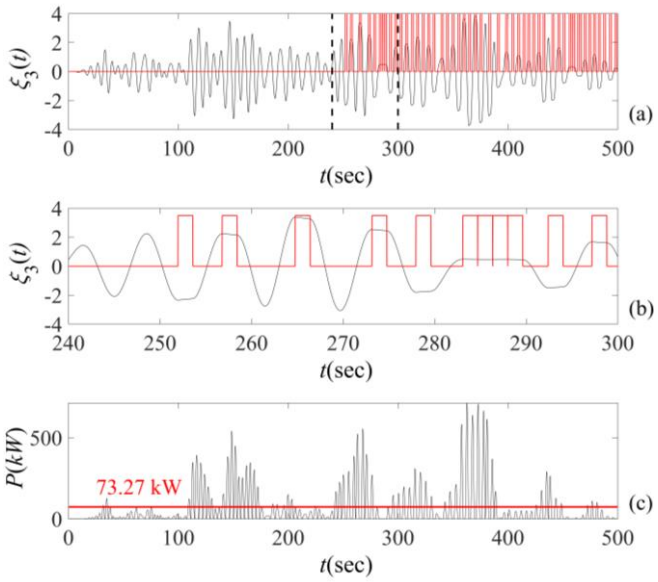

Fig. 13. (a, b) Heaving Motion and Latching Windows for Cyl-WEC a/h=0.225, T/h=0.45, B_{PTO}=10x $B_{33,av}$ and C_{PTO}=0.1xC_{33}. (c) Power Absorption. h=20m, T_p=10s, H_s=2m.

Results show that, with latching control, the WEC is able to achieve mean wave power absorption of about 73.2 *kW*, versus 58.2 *kW* without latching, corresponding to a 25.8% increase. It is noted that steady state conditions are ensured by calculating the average power absorption after 50% of the complete time span.

Another latching approach also focuses on prediction of the exact moment of the next peak in excitation force and declutching of the device a quarter of the resonance period before this moment [23]. However, this to be investigated in future work, along with other ways of improving latching control while maintaining the computational cost reasonable.

V. Conclusion

In the present study a full 3D model based on Boundary Element Method has been developed to treat the hydrodynamic problem of a WEC's installation at the exposed side of a breakwater. Assuming different characteristics of the PTO and different angles of propagation of the incident field, the results manifest significant increase of harnessed power from the device, due to the presence of the wall. In continuation and aiming to address another aspect of wave energy research, a time-domain model is developed for the implementation of latching control, based on a Predictor-Corrector numerical integration algorithm. The subject case, scaled at realistic dimensions of the WEC and wave spectrum characteristics, presents a 25.8% increase in levels of power absorption in case of applying the control, compared to the initial system. Based on the present research, areas for future work are also identified, with the main item upon further investigation being the consideration of high sea spectrum irregularities and extension to the treatment of the latching control including the wall's effects, which is expected to provide more auspicious results in terms of power extraction. Next step could also be evaluations regarding a WEC array layout where more complicated fluid structure interactions, including wall effects and arbitrary bottom topography, require more sophisticated control strategies. The above could be also approached by the MMSE model [5] for significant computational cost reduction, given that using the present layout requires discretization of multiple WECs, an extended free surface area and the vertical wall.

References

[1] K. A. Belibassakis, M. Bonovas and E. Rusu, "A Novel Method for Estimating Wave Energy Converter Performance in Variable Bathymetry Regions and Applications, " *Energies* 11(8):2092, 2018.

[2] V. Stratigaki, P. Troch, T. Stallard, D. Forehand, J. P. Kofoed, M. Folley, M. Benoit, A. Babarit and J. Kirkegaard, "Wave Basin Experiments with Large Wave Energy Converter Arrays to Study Interactions between the Converters and Effects on Other Users in the Sea and the Coastal Area," *Energies*, vol. 7, pp. 701-734, 2014.

[3] F. Charrayre, C. Peyrard, M. Benoit and A. Babarit, "A coupled methodology for wave body interactions at the scale of a farm of wave energy converters including irregular bathymetry," in *33rd Intern. Conference on Offshore Mechanics and Arctic Engineering (OMAE2014),* San Francisco, 2014.

[4] P. McCallum, V. Venugopal, D. Forehand and R. Sykes, "On the performance of an array of floating energy converters for different water depths," in *33rd Intern. Conference on Offshore Mechanics and Arctic Engineering (OMAE2014),* San Francisco, 2014.

[5] M. Bonovas, A. Magkouris and K. Belibassakis, "A Modified Mild-Slope Model for the Hydrodynamic Analysis of Arrays of Heaving WECs in Variable Bathymetry Regions," *Fluids* (7) 183, 2022. DOI: 10.3390/fluids7060183.

[6] S.R. Massel, "Ocean surface waves. Their physics and prediction," Singapore, World Scientific, 2013.

[7] P.G. Chamberlain and D. Porter, "The modified mild-slope equation", *Journal of Fluid Mechanics*. vol. 291, pp. 393-407, 1995.

[8] K.A. Belibassakis, "A Boundary Element Method for the hydrodynamic analysis of floating bodies in general bathymetry regions," *Engineering Analysis with Boundary Elements*, vol. 32, pp. 796-810, 2008.

[9] K. Belibassakis, M. Bonovas and E. Rusu, "A Novel Method for Estimating Wave Energy Converter Performance in Variable Bathymetry Regions and Applications," *Energies* 11(8):2092, 2018. DOI: 10.3390/en11082092.

[10] M. Bonovas, K.A. Belibassakis and E. Rusu, "Multi-DOF WEC Performance in Variable Bathymetry Regions Using a Hybrid 3D BEM and Optimization", *Energies* 12:2108. 2019. DOI: 10.3390/en12112108.

[11] J. Katz and A. Plotkin, "Low speed aerodynamics," McGraw-Hill, 2001.

[12] J. Newman, "Distributions of sources and normal dipoles over a quadrilateral panel," *Journal of Engineering Mathematics* vol. 20, pp. 113-126, 1986.

[13] A. Babarit, A.H. Clément, "Optimal latching control of a wave energy device in regular and irregular waves," *Applied Ocean Research* vol. 28,(2), pp. 77-91, 2006, DOI: https://doi.org/10.1016/j.apor.2006.05.002.

[14] K. Budal, J. Falnes, T. Hals, L.C. Iversen and T. Onshus, "Model experiment with a phase-controlled point absorber," in *Second International Symposium on Wave and Tidal Energy*, Cambridge, UK, pp 191-206, 1981.

[15] J. Hals, J. Falnes and T. Moan, "Constrained optimal control of a heaving buoy wave-energy converter," *Journal of Offshore Mechanics and Arctic Engineering* vol. 133(1), 2011.

[16] M. Bonovas and I. Anagnostopoulos, "Modelling of operation and optimum design of a wave power take-off system with energy storage," *Renewable Energy* vol. 141, pp. 502-514. 2019. DOI: 10.1016/j.renene.2019.08.101.

[17] R. Yeung, "Added mass and damping of a vertical cylinder in finite depth waves," *Applied Ocean Research* vol. 3, pp. 119-133, 1981.

[18] T. Sabuncu, and S Calisal, "Hydrodynamic coefficients for vertical circular cylinders at finite depth," *Ocean Engineering* vol. 8, pp. 25-63, 1981.

[19] C. J. R. Garrett, "Wave forces on a circular dock," *Journal of Fluid Mechanics* vol. 46(1), pp. 129 – 139, 1971, DOI: :10.1017/S0022112071000430.

[20] J Black, C. Mei and M Bray, "Radiation and scattering of water waves by rigid bodies," *Journal of Fluid Mechanics* vol 46(1), pp. 151-164. 1971. DOI: 10.1017/S0022112071000454.

[21] E. Anderlini, D. I. M. Forehand, E. Bannon, Q. Xiao and M Abusara, "Reactive control of a two-body point absorber using reinforcement learning," *Ocean Engineering* vol. 148, pp. 650-658, 2018. ISSN 0029-8018.

[22] M. Peñalba, A. Merigaud, J. C. Gilloteaux and J. V. Ringwood, "Nonlinear Froude-Krylov force modelling for two heaving wave energy point absorbers," in *11th European Wave and Tidal Energy Conference*, Nantes, France, 2015.

[23] R. G. Coe, G. Bacelli, D. G. Wilson, O. Abdelkhalik, U.A. Korde and R.D. Robinett, "A comparison of control strategies for wave energy converters,"*International Journal of Marine Energy* vol. 20, pp.45-63, 2017. DOI: https://doi.org/10.1016/j.ijome.2017.11.001.